HHS Public Access

Author manuscript

*Int J Radiat Oncol Biol Phys*. Author manuscript; available in PMC 2015 October 01.

Published in final edited form as:

*Int J Radiat Oncol Biol Phys*. 2014 October 1; 90(2): 376–384. doi:10.1016/j.ijrobp.2014.03.049.

# Volumetric Spectroscopic Imaging of Glioblastoma Multiforme Radiation Treatment Volumes

**N. Andres Parra, PhD**[*], **Andrew A. Maudsley, PhD**[†], **Rakesh K. Gupta, MD**[‡], **Fazilat Ishkanian, MD**[*], **Kris Huang, MD**[*], **Gail R. Walker, PhD**[§], **Kyle Padgett, PhD**[*,†], **Bhaswati Roy, PhD**[‡], **Joseph Panoff, MD**[*], **Arnold Markoe, MD**[*], and **Radka Stoyanova, PhD**[*]

[*]Department of Radiation Oncology, University of Miami Miller School of Medicine, Miami, Florida

[†]Department of Radiology, University of Miami Miller School of Medicine, Miami, Florida

‡Department of Radiology & Imaging, Fortis Memorial Research Institute, Gurgaon, Haryana, India

[§]Department of Biostatistics and Bioinformatics Core Resource, Sylvester Cancer Center, University of Miami Miller School of Medicine, Miami, Florida

## Abstract

**Purpose—**Magnetic resonance (MR) imaging and computed tomography (CT) are used almost exclusively in radiation therapy planning of glioblastoma multiforme (GBM), despite their well-recognized limitations. MR spectroscopic imaging (MRSI) can identify biochemical patterns associated with normal brain and tumor, predominantly by observation of choline (Cho) and *N*-acetylaspartate (NAA) distributions. In this study, volumetric 3-dimensional MRSI was used to map these compounds over a wide region of the brain and to evaluate metabolite-defined treatment targets (metabolic tumor volumes [MTV]).

**Methods and Materials—**Volumetric MRSI with effective voxel size of ~1.0 mL and standard clinical MR images were obtained from 19 GBM patients. Gross tumor volumes and edema were manually outlined, and clinical target volumes (CTVs) receiving 46 and 60 Gy were defined ($CTV_{46}$ and $CTV_{60}$, respectively). $MTV_{Cho}$ and $MTV_{NAA}$ were constructed based on volumes with high Cho and low NAA relative to values estimated from normal-appearing tissue.

**Results—**The MRSI coverage of the brain was between 70% and 76%. The $MTV_{NAA}$ were almost entirely contained within the edema, and the correlation between the 2 volumes was significant (r=0.68, *P*=.001). In contrast, a considerable fraction of $MTV_{Cho}$ was outside of the edema (median, 33%) and for some patients it was also outside of the $CTV_{46}$ and $CTV_{60}$. These untreated volumes were greater than 10% for 7 patients (37%) in the study, and on average more than one-third (34.3%) of the $MTV_{Cho}$ for these patients were outside of $CTV_{60}$.



Reprint requests to: Radka Stoyanova, PhD, Department of Radiation Oncology, University of Miami Miller School of Medicine, Hope Lodge, Suite 307, 1121 NW 14th St, Miami, FL 33136. Tel: (305) 243-5856; RStoyanova@med.miami.edu.

Conflict of interest: none.

Supplementary material for this article can be found at www.redjournal.org.

**Conclusions—**This study demonstrates the potential usefulness of whole-brain MRSI for radiation therapy planning of GBM and revealed that areas of metabolically active tumor are not covered by standard RT volumes. The described integration of MTV into the RT system will pave the way to future clinical trials investigating outcomes in pa tients treated based on metabolic information.

## Introduction

Current practice for radiation therapy (RT) of glioblastoma multiforme (GBM) uses T1-weighted, gadolinium enhanced, fluid attenuation inversion recovery (FLAIR) and/or T2-weighted magnetic resonance imaging (MRI) to define target volumes. Two target volumes are defined, where 46 Gy is prescribed to a larger volume that includes contrast-enhancing tumor and/or surgical cavity (gross tumor volume [GTV]), and the region indicated by the FLAIR/T2 abnormality (edema), with an additional 2-cm margin (clinical tumor volume 46 [$CTV_{46}$]). The second volume includes the GTV with a margin of 2 to 2.5 cm and receives a boost to an additional 14 Gy for a total dose of 60 Gy ($CTV_{60}$). The CTVs for GBM are based on the 1980 study by Hochberg and Pruitt (1) that showed, using computed tomography (CT), 78% of recurrences of GBM were within 2 cm of the margin of the initial tumor bed and 58% were within 1 cm. Additional studies have confirmed that the majority of recurrences appear within the high-dose regions of current RT plans (2-4). Based on MRI, it is now accepted that 90% of all GBM recurrences occur 2 to 3 cm from the tumor margins.

MRI and CT are almost exclusively used for RT planning of GBM; yet the limitations of these structural imaging modalities with regard to characterizing tumor infiltration and tissue viability are recognized. Histological investigations have shown tumor cells in the surrounding edema and in the adjacent normal-appearing brain that are not associated with any radiographic findings (5); hence, there may be tumor cells left outside of the treatment fields. Conversely, areas with radiological abnormalities may not contain any tumor cells, resulting in normal brain tissue in the treatment volume and unnecessarily increasing toxicity.

Unlike standard MRI, proton ($^1$H) magnetic resonance spectroscopy (MRS) has the ability to characterize biochemical patterns associated with normal brain, tumor histopathology, and changes in tissue function, thereby providing indicators for the diagnosis, classification, and progression of disease in the brain (6-8). MRS can detect several metabolites in vivo, in particular choline (Cho) and *N*-acetylaspartate (NAA), which have been strongly associated with primary brain tumors (6). Cho is a marker of increased cell membrane proliferation and is increased in brain tumors (6, 7). High levels of NAA are a marker of mature neuronal density and viability, and are therefore decreased in tumor tissue where the neuronal cell density is reduced (6, 7, 9).

MRS imaging (MRSI), which enables MRS acquisition from multiple volumes covering a region of the brain, has shown great promise to identify areas of metabolic activity and to guide the radiation oncologist in targeting malignant regions (10-12). Encouraging results from current phase 2 trial of radiosurgery to MRSI-defined high-risk tumor volumes in

patients with GBM were recently published (13). In another study, MRSI was integrated into treatment planning system for GBM using dose painting with integrated simultaneous boost (14). It should be noted that in these studies, MRSI covered only part of the brain/tumor.

In this report, volumetric 3-dimensional (3D) MRSI acquisition was used, which included sampling of the entire brain volume to carry out a comprehensive assessment of metabolically suspicious areas. Metabolic tumor volumes (MTVs) are translated into a Radiation Workstation and compared with standard RT volumes for GBM.

## Methods and Methods

### MRSI acquisition and analysis

A total of 19 treatment-naive patients (13 men and 6 women, aged 30-69 years, mean 49 years) (Table 1) with postimaging histopathologically confirmed GBM were retrospectively reviewed from a larger imaging glioma study (15).

The comprehensive imaging studies (pre- and post-contrast T1; T2-weighted, perfusion, and diffusion MRI) were carried out on a 3T Signa (GE, Milwaukee, WI) as described in detail elsewhere (15). MRSI data were obtained using a volumetric acquisition resulting in full coverage of the brain with field of view (FOV) 280 × 280 × 180 $mm^3$ and 64 × 64 × 32 voxels with effective voxel size ~1.0 mL (16). A second MRSI dataset from the water signal, referred to as the “water reference,” was acquired simultaneously in an interleaved fashion and with parameters identical to those for the metabolite MRSI signal.

Imaging and spectroscopy data were processed using the Metabolite Imaging and Data Analysis System (MIDAS) package (17). Although a number of processing steps are used for the MRSI reconstruction, those relevant for this project are summarized in Figure 1A. T1-based brain segmentation was carried out using automatic brain segmentation tool/library FSL/FAST (18). First, the metabolite signal was quantified by using an automated parametric spectral analysis procedure (19), with a Gaussian lineshape model and basis functions for the metabolite spectra obtained by spectral simulation (20). Second, the spectral analysis was followed by a simple quality evaluation procedure that created a “quality image” that reflects areas of MRSI with water linewidth of ≤20 Hz. This image, $MRSI_Q$, was used as a mask for excluding from further consideration image regions with suboptimal spectral quality (Fig. 1A, spectral quality mask). The water map was used for fusion of the MRSI with the subject T1 MRI, which was done in the radiation treatment software MIM (MIM Software Inc., Cleveland, OH) (Fig. 1A, registration box), and this transformation applied to the metabolite maps from MRSI analysis. Third, the individual metabolite concentrations (Cho, Creatine [Cre], and NAA) were normalized using tissue water as an internal reference. The effect of partial volume of cerebrospinal fluid (CSF) on the metabolite relative concentrations in the normal tissue region was also corrected for, as CSF content dilutes the real metabolite concentration (Fig. 1A, tissue segmentation and metabolic maps) (18).

### Radiation treatment volumes and metabolic tumor volumes

GTV was defined on postcontrast T1-weighted images and included all areas of contrast enhancement. $CTV_{46}$ was defined as GTV+FLAIR/T2 abnormality plus a 2-cm circumferential margin. Here, and in the rest of this article, we will refer to the FLAIR/T2 abnormality as "edema." $CTV_{60}$ was defined as the GTV+2.5 cm circumferential margin. Contouring was done by a single radiation oncolo-gist, and the CTVs were automatically calculated using MIM (Fig. 1, top right-hand block, shaded green).

The direct measurement of relative concentration (in institutional units [i.u.]) of Cho and NAA was used to determine the pertinent areas of infiltrating/aggressive disease (21). Normal-appearing tissue (NAT) were areas outside of ($CTV_{60}$+2.5 cm)U($CTV_{46}$+2 cm). Because the distributions of Cho/NAA in NAT failed the Kolmogorove–Smirnov test for normality, extreme values were not well characterized by distance from the mean expressed as a multiple of the standard deviation. Instead, maps of aberrant high Cho ($MTV_{Cho}$) and low NAA ($MTV_{NAA}$) were constructed using threshold values set for each patient by applying Tukey's rule to identify outlier values from the metabolite distribution in NAT (22). Before this calculation, the cerebellum, brainstem, and ventricles were excluded from the NAT calculations because of their specific metabolic signatures (Fig. 1, normal-appearing tissue box).

The relationships between RT volumes and MRSI-derived MTVs were investigated using the MIM toolbox for volume comparisons. In particular, the fractions of $MTV_{Cho}$ and $MTV_{NAA}$ outside of GTV, edema, $CTV_{60}$, and $CTV_{46}$ were calculated.

## Results

The analysis pipeline for comparison of metabolic and RT target volumes is displayed in Figure 1A. The MRSI was co-registered with the MRI in MIDAS (17); but nevertheless, for generalization of the workflow, the water reference map was fused with the T1 MRI. Indeed, the transformation parameters were small: mean translation/rotation in (x,y,z): 0.29, 1.46, and 1.15 mm/0.36 °, 2.04 °, and 0.81°, respectively. Figures 1B and 1C illustrate the delineation of brain structures (cerebellum and brain stem) and CSF, as well as the RT target volumes. Although the data are acquired from the entire brain, a number of spectra, mainly in the frontal part of the brain, are eliminated because of poor quality. The MRSI coverage of the brain, $MRSI_Q$, is depicted in light blue in Figure 1B. The brain and $MRSI_Q$ volumes (Table 1, columns 4 and 9) indicate that the MRSI coverage of the brain was between 70% and 76% (median 74%). The median percentage of coverage of the RT volumes were 89%, 85%, 81%, and 79% for GTV, edema, $CTV_{60}$, and $CTV_{46}$. To assess the limitation of MRSI for full coverage of the RT targets based on tumor location (superior/inferior, anterior/posterior), the fractions of the RT volumes outside of the $MRSI_Q$ were calculated (Fig. 1D). Tumors in the frontal part of the brain have limited coverage, with about 20% to 30% of the CTVs located outside of the spectroscopy assessment volume.

"Normal" metabolite values were estimated in the NAT (Fig. 1C, purple) and box plots of Cho and NAA distributions are shown in Supplemental Figure 1. Considerable variation was found among patients with respect to Cho, NAA, and Cr (data not shown) in NAT; the

coefficient of variation (CV) was 22%, 15%, and 17%, respectively. The CV for Cho, however, was higher than for the other 2 metabolites, indicating that additional covariates other than the common experimental and physiological may be contributing to Cho. The vertical bars in the plots indicate thresholds (or inner fences), above/below which values are considered to be outliers by Tukey's rule (22). $MTV_{Cho}$ consists of pixels with Cho concentrations above the upper fence in the Cho graph, and the pixels in $MTV_{NAA}$ are below the lower fence on the NAA.

An example of the construction of the metabolic volumes is shown in Figure 2. A portion of the axial T1 post–contrast MRI from patient T7 is overlaid with the spectral data; representative spectra (Fig. 2B) from normal brain, edema, and enhancing lesion are shown in the column to the right, which illustrate Cho amplitude increasing and reaching the highest values in GTV, whereas NAA is absent in this region. $MTV_{Cho}$ depicting areas of high Cho (blue) and $MTV_{NAA}$ (purple) are shown in Figure 2C. The $MTV_{NAA}$ conforms almost entirely to the edema seen on the T2-weighted MRI, whereas 93%, 25%, 16%, and 3% of $MTV_{Cho}$ are outside of the GTV, edema, $CTV_{60}$, and $CTV_{46}$, respectively. In Figure 3, a portion of the T2-weighted MRI is shown from patient T1, overlaid with the corresponding spectral data. Here Cho is the highest outside of enhancing lesion and the edema. Figure 3B again demonstrates strong overlap of $MTV_{NAA}$ (purple) and the edema, whereas $MTV_{Cho}$ (blue) extends outside of GTV and the edema region. The blue region appears more anteriorly on the metabolic map in comparison with the T2 MRI, because edge voxels are commonly removed due to poor quality and lipid contamination. Figure 4 shows an example of a larger tumor T15 with a necrotic center and variable metabolic content in the edema. The spectra from within the edema region at the top and leftmost regions of the image in Figure 4A are characterized by high Cho, whereas the one at the upper left shows reduced content for all metabolites. The spectrum at the lower left has “normal” Cho values. In this example, the GTV contains mostly necrotic tissue. Figure 4C shows the $MTV_{Cho}$ location along 3 orthogonal directions to illustrate the extent of the tumor and the 3D MRSI–derived information. In this example, $MTV_{NAA}$ again conforms to the edema (data not shown). In Figure 5, coronal views of $MTV_{Cho}$ and $MTV_{NAA}$ are shown for patient T6, with these overlaid on the T1 postcontrast (Fig. 5C). There was no discernible edema in this patient's MRIs. The high Cho in this case corresponds to the enhancing portions of the lesion that surround a necrotic center.

The RT and metabolic volumes are summarized in Table 1. As shown in the examples, $MTV_{NAA}$ are almost entirely contained within the edema. Indeed, a small fraction of $MTV_{NAA}$ (with median of 8%) is outside of the edema. In addition, the correlation between the 2 volumes ($MTV_{NAA}$ and edema) is significant ($r=0.68$, $P=.001$; Fig. 5D). In contrast, a considerable fraction of $MTV_{Cho}$ is outside of the edema (median 33%). More importantly, large fractions of $MTV_{Cho}$ for some of the patients are also outside $CTV_{46}$ and/or $CTV_{60}$ (Fig. 5E). For 7 patients (37%) in the study, these untreated volumes were greater than 10% of the proposed $MTV_{Cho}$, with an average 34.4% of $MTV_{Cho}$ outside of $CTV_{60.}$ In addition, 4 of these 7 patients, as well as 1 patient with 7.4% $MTV_{Cho}$ outside $CTV_{60,}$ had more than 10% $MTV_{Cho}$ outside of $CTV_{46}$.

## Discussion

In this work, we describe a unique approach to semi-automatic delineation of target tumor volumes based on 3D MRSI in patients with GBM. The value of spectroscopy to guide RT planning has been discussed in previous reports (11, 12, 14,23-25); however, this is the first study to make use of whole-brain volumetric 3D MRSI. A limitation of previously published evaluations has been the use of preselected FOV of MRSI that represented only partial brain volumes. For example, the MRSI "box" in Ozturk-Isik et al (11) is on a 12 × 12 × 8 grid with a FOV of 120 × 120 × 80 $mm^3$, and the reported median percentage of the edema within the FOV was 54.2%, whereas the corresponding number for this report is 83.7%. The increased coverage leads to better characterization of normal and abnormal tissues, and a more accurate representation of the target volumes. In a report from Ken et al (14), describing the integration of 3D MRSI with a treatment planning system, data were collected using 16 × 16 × 8 points over a FOV of 100 × 100 × 20 $mm^3$. The FOV was positioned over the tumor to cover the majority of abnormalities, while avoiding regions of bone and subcutaneous lipids that could corrupt the spectra. The use of the whole-brain acquisition avoids the need to manually position the MRSI volume, thereby enabling better sampling of both tumor and normal tissue regions without selection bias and with better visualization of the metabolically active tumor throughout the patient's brain. Conformal and full coverage of the brain and tumor regions is essential for spectroscopy findings to have an impact on RT plans.

Whole-brain MRSI sampling brings several limitations to the forefront, notably the effect of field inhomogeneity in the inferior temporal and frontal regions that may limit spectroscopic characterization in tumors located in these regions. As shown in Figure 1D, on average, more than 25% of GTV of frontal and anterior tumors are outside of the MRSI. In addition, MRSI requires longer acquisition times (~25 minutes) that may not be tolerated by all patients and may lead to motion artifacts that limit the quality of the data acquired. To account for variability in spectral quality, an automatic quality evaluation procedure was used that excluded voxels with inadequate spectral quality. On average, 30% of voxels per patient were excluded. Tumor location, variable spectral quality, and possible errors introduced by the threshold for differentiating normal from cancerous tissue resulted in a couple of negligible $MTV_{Cho}$ (Table 1, T13 and T16).

The goal of the current analytic procedure was to determine areas of active and infiltrating tumor. Unlike previous reports in which Cho was normalized to NAA, either as Choto-NAA ratio (26) or Cho-to-NAA index (7, 27), only the magnitude of Cho, normalized by tissue water signal, were used to identify areas suspicious for tumor activity. High levels of Cho are associated with membrane proliferation and tumor aggressiveness, and recent studies emphasize the complex reciprocal interactions between oncogenic signaling and Cho metabolism (28). The mapping of the $MTV_{NAA}$ and $MTV_{Cho}$ suggests that the reduction of NAA may be secondary in the process of tumorigenesis; therefore, it is proposed that using Cho signals alone may be more accurate in depicting active disease. The $MTV_{NAA}$ volumes determined in this study were found to conform closely with the edema, potentially suggesting that NAA alone does not lead to differential volumes compared to the ones obtained from conventional MRI. On the other hand, $MTV_{Cho}$ distributions have great

variability among GBM patients. The spectroscopic content of the enhancing lesions, which may appear very similar on MRI, vary from high Cho, reduced values, and even areas completely void of metabolites. This also results in variable spectral quality, as shown in Figures 3 and 4. The edema is even more metabolically heterogeneous among patients, possibly because of some areas including tumor infiltration and other areas representing edema without active tumor. In a few cases, high Cho regions were found outside of the GTV and edema altogether, and it was shown that 37% of patients studied had metabolically active tumor outside $CTV_{60.}$ Therefore, a significant portion of patients were found to have disease that fell outside of the high-dose RT volumes. Furthermore, not all edema areas may represent microscopic active disease, and a portion of the $CTV_{46}$ will treat normal brain. $MTV_{Cho}$ also shows heterogeneous signals inside the GTV, which indicate areas that are more metabolically active and could be targeted for dose escalation or other targeted treatments.

The contribution of these findings for improving RT outcomes can be determined only in the framework of a clinical trial. Integrating MTV into our current RT system, provided that metabolic information is seamlessly available for defining radiation targets, will pave the way to such trials investigating outcomes in patients treated based on the incorporated metabolic information. The presented approach captures a snapshot of the metabolic status of a tumor in 3D volumes, and this information may lead to the development of novel treatment strategies tailored to each patient's active tumor. Individualized target volumes based on metabolically active disease, rather than the simple circumferential CTV margins, may permit a reduction of normal brain volumes treated unnecessarily as well as dose escalation and better target definition.

## Supplementary Material

Refer to Web version on PubMed Central for supplementary material.

## Acknowledgments

This publication was supported by grant 10BN03 from Bankhead Coley Cancer Research Program, R01EB000822 from the National Cancer Institute, and award 20-2009 from the Indo-US Science & Technology Forum.

## References

1. Hochberg FH, Pruitt A. Assumptions in the radiotherapy of glioblastoma. Neurology. 1980; 30:907–911. [PubMed: 6252514]
2. Chang EL, Akyurek S, Avalos T, et al. Evaluation of peritumoral edema in the delineation of radiotherapy clinical target volumes for glioblastoma. Int J Radiat Oncol Biol Phys. 2007; 68:144–150. [PubMed: 17306935]
3. Lee SW, Fraass BA, Marsh LH, et al. Patterns of failure following high-dose 3-D conformal radiotherapy for high-grade astrocytomas: A quantitative dosimetric study. Int J Radiat Oncol Biol Phys. 1999; 43:79–88. [PubMed: 9989517]
4. Oppitz U, Maessen D, Zunterer H, et al. 3D-recurrence-patterns of glioblastomas after CT-planned postoperative irradiation. Radiother Oncol. 1999; 53:53–57. [PubMed: 10624854]
5. Burger PC, Dubois PJ, Schold SC Jr, et al. Computerized tomographic and pathologic studies of the untreated, quiescent, and recurrent glioblastoma multiforme. J Neurosurg. 1983; 58:159–169. [PubMed: 6294260]

6. Dowling C, Bollen AW, Noworolski SM, et al. Preoperative proton MR spectroscopic imaging of brain tumors: Correlation with histopathologic analysis of resection specimens. AJNR Am J Neuroradiol. 2001; 22:604–612. [PubMed: 11290466]
7. McKnight TR, von dem Bussche MH, Vigneron DB, et al. Histo-pathological validation of a three-dimensional magnetic resonance spectroscopy index as a predictor of tumor presence. J Neurosurg. 2002; 97:794–802. [PubMed: 12405365]
8. Garcia-Gomez JM, Luts J, Julia-Sape M, et al. Multiproject-multi-center evaluation of automatic brain tumor classification by magnetic resonance spectroscopy. Magn Reson Materials Phys Biol Med. 2009; 22:5–18.
9. Moffett JR, Namboodiri MA, Cangro CB, et al. Immunohistochemical localization of N-acetylaspartate in rat brain. Neuroreport. 1991; 2:131–134. [PubMed: 1768855]
10. Nelson SJ, Graves E, Pirzkall A, et al. In vivo molecular imaging for planning radiation therapy of gliomas: An application of 1H MRSI. J Magn Reson Imaging. 2002; 16:464–476. [PubMed: 12353260]
11. Ozturk-Isik E, Pirzkall A, Lamborn KR, et al. Spatial characteristics of newly diagnosed grade 3 glioma assessed by magnetic resonance metabolic and diffusion tensor imaging. Transl Oncol. 2012; 5:10–18. [PubMed: 22348171]
12. Park I, Tamai G, Lee MC, et al. Patterns of recurrence analysis in newly diagnosed glioblastoma multiforme after three-dimensional conformal radiation therapy with respect to pre-radiation therapy magnetic resonance spectroscopic findings. Int J Radiat Oncol Biol Phys. 2007; 69:381–389. [PubMed: 17513061]
13. Einstein DB, Wessels B, Bangert B, et al. Phase II trial of radiosurgery to magnetic resonance spectroscopy-defined high-risk tumor volumes in patients with glioblastoma multiforme. Int J Radiat Oncol Biol Phys. 2012; 84:668–674. [PubMed: 22445005]
14. Ken S, Vieillevigne L, Franceries X, et al. Integration method of 3D MR spectroscopy into treatment planning system for glioblastoma IMRT dose painting with integrated simultaneous boost. Radiat Oncol. 2013; 8:1. [PubMed: 23280007]
15. Roy B, Gupta RK, Maudsley AA, et al. Utility of multiparametric 3-T MRI for glioma characterization. Neuroradiology. 2013; 55:603–613. [PubMed: 23377234]
16. Chawla S, Wang S, Kim S, et al. Radiation injury to the normal brain measured by 3D-echo-planar spectroscopic imaging and diffusion tensor imaging: Initial experience. J Neuroimaging. 2013; 00:1–8.
17. Maudsley AA, Darkazanli A, Alger JR, et al. Comprehensive processing, display and analysis for in vivo MR spectroscopic imaging. NMR Biomed. 2006; 19:492–503. [PubMed: 16763967]
18. Zhang YY, Brady M, Smith S. Segmentation of brain MR images through a hidden Markov random field model and the expectation-maximization algorithm. IEEE Transact Med Imaging. 2001; 20:45–57.
19. Soher BJ, Young K, Govindaraju V, et al. Automated spectral analysisdIII: Application to in vivo proton MR spectroscopy and spectroscopic imaging. Magn Reson Med. 1998; 40:822–831. [PubMed: 9840826]
20. Soher BJ, Young K, Bernstein A, et al. GAVA: Spectral simulation for in vivo MRS applications. J Magn Reson. 2007; 185:291–299. [PubMed: 17257868]
21. Haddadin IS, McIntosh A, Meisamy S, et al. Metabolite quantification and high-field MRS in breast cancer. NMR Biomed. 2009; 22:65–76. [PubMed: 17957820]
22. Tukey, JW. Exploratory Data Analysis. Addison-Wesley; Reading, MA: 1977.
23. Chan AA, Lau A, Pirzkall A, et al. Proton magnetic resonance spectroscopy imaging in the evaluation of patients undergoing Gamma knife surgery for grade IV glioma. J Neurosurg. 2004; 101:467–475. [PubMed: 15352605]
24. Pirzkall A, Li X, Oh J, et al. 3D MRSI for resected high-grade gliomas before RT: Tumor extent according to metabolic activity in relation to MRI. Int J Radiat Oncol Biol Phys. 2004; 59:126–137. [PubMed: 15093908]
25. Chernov MF, Hayashi M, Izawa M, et al. Multivoxel proton MRS for differentiation of radiation-induced necrosis and tumor recurrence after gamma knife radiosurgery for brain metastases. Brain Tumor Pathol. 2006; 23:19–27. [PubMed: 18095115]

26. Wijnen JP, Idema AJ, Stawicki M, et al. Quantitative short echo time 1H MRSI of the peripheral edematous region of human brain tumors in the differentiation between glioblastoma, metastasis, and meningioma. J Magn Reson Imaging. 2012; 36:1072–1082. [PubMed: 22745032]

27. McKnight TR, Noworolski SM, Vigneron DB, et al. An automated technique for the quantitative assessment of 3D-MRSI data from patients with glioma. J Magn Reson Imaging. 2001; 13:167–177. [PubMed: 11169821]

28. Glunde K, Bhujwalla ZM, Ronen SM. Choline metabolism in malignant transformation. Nat Rev Cancer. 2011; 11:835–848. [PubMed: 22089420]

## Summary

Metabolic volumes based on volumetric magnetic resonance spectroscopic imaging are compared with standard radiation therapy volumes in 19 treatment-naive glioblastoma multiforme patients. Volumes related to active and infiltrative tumor were outside of the treatment area in one-third of them. This is the first comprehensive evaluation of magnetic resonance spectroscopic imaging covering the entire brain. The data are integrated in radiation therapy software and may lead to the development of novel treatment strategies tailored to each patient's active tumor.

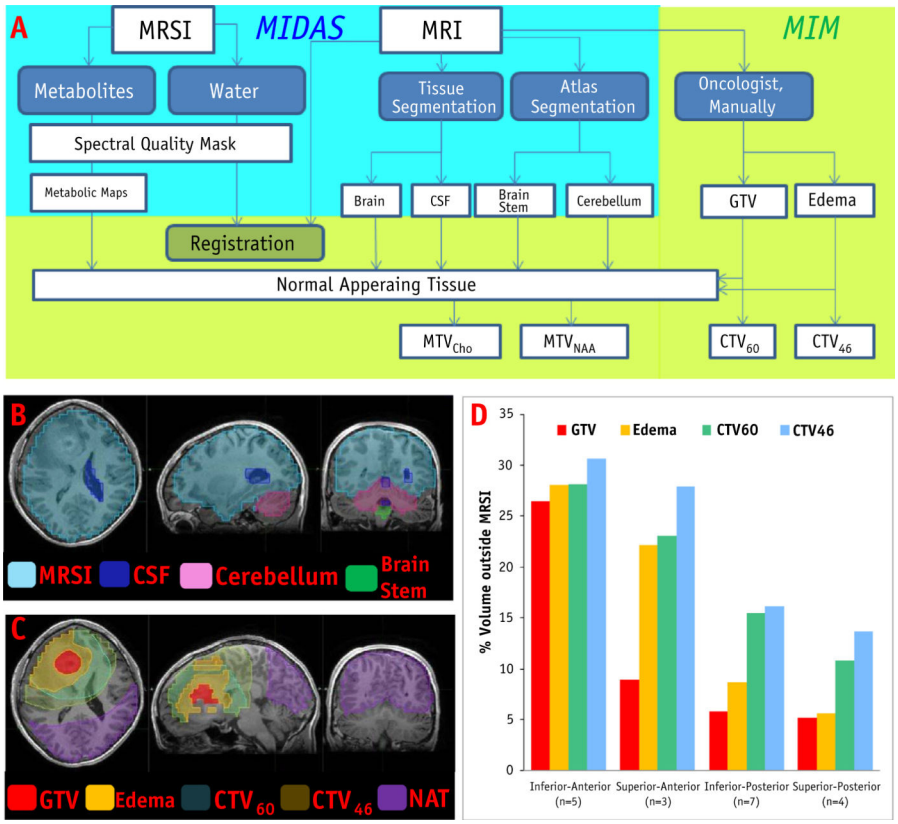


**Fig. 1.**

(A) Schema of workflow. Upper left-hand side (shaded in blue) denotes the steps carried out in MIDAS. Registration, radiation therapy (RT) volume contouring, and comparisons with metabolic tumor volumes (MTV) were performed with the MIM system. (B) Spectral quality mask (light blue), cerebrospinal fluid (CSF; dark blue), and brain segmentation (cerebellum and brainstem). (C) RT volumes and area of normal-appearing tissue (NAT). (D) RT volumes outside of the volume of magnetic resonance spectroscopic imaging within the "quality mask" ($MRSI_Q$) based on tumor location. A color version of this figure available at www.redjournal.org.

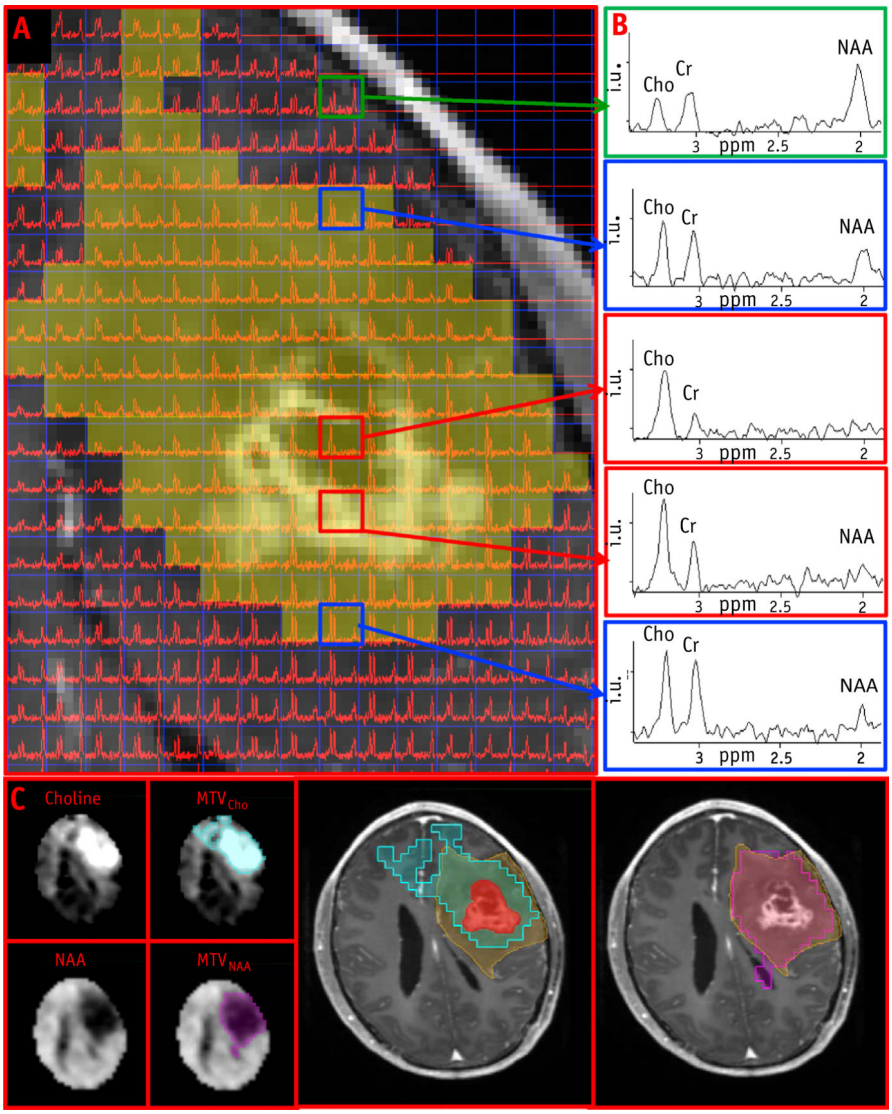


**Fig. 2.**

(A) Magnetic resonance spectroscopic imaging (MRSI) data from the tumor region overlaid on the postcontrast T1. Shaded area indicates region of high choline. (B) Representative spectra from top: normal tissue, edema, lesion and enhancing edge, and edema. (C) Choline (Cho) and *N*-acetylaspartate (NAA) maps in the axial slice in (A). Blue and purple areas indicate $MTV_{Cho}$ and $MTV_{NAA}$. GTV (red), edema (orange) and $MTV_{Cho}$ overlaid on T1-weighted MRI. MTV Z metabolic tumor volumes. A color version of this figure available at www.redjournal.org.

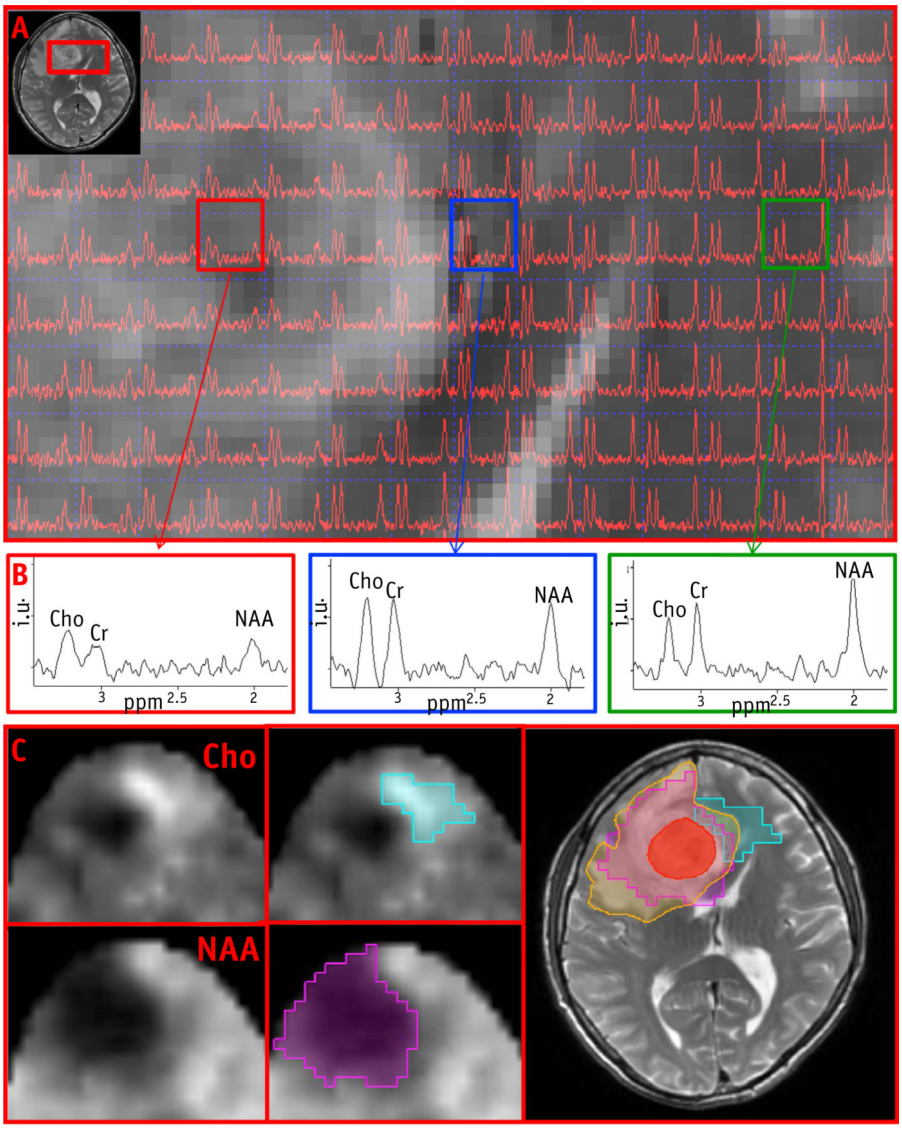


**Fig. 3.**

(A) Magnetic resonance spectroscopic imaging (MRSI) data from the tumor region, indicated by the red box on T2-MRI (inset). (B) Representative spectra from gross tumor volume (GTV), outside GTV/edema and normal-appearing tissue (NAT; green box). (C) Choline (Cho) and *N*-acetylaspartate (NAA) maps around region from A. Blue and purple areas indicate $MTV_{Cho}$ and $MTV_{NAA}$. GTV (red) and edema (orange) overlaid on T2-MRI and metabolic volumes. MTV = metabolic tumor volumes. A color version of this figure available at www.redjournal.org.

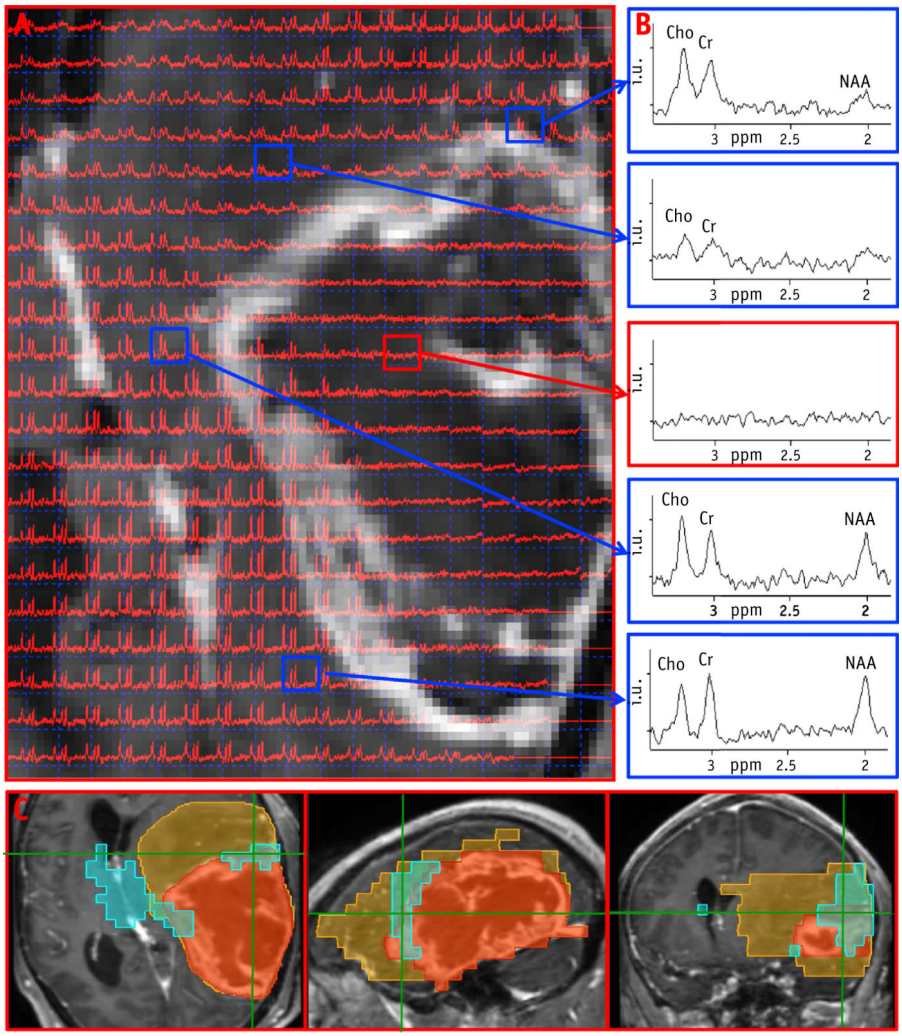


**Fig. 4.**

(A) Magnetic resonance spectroscopic imaging (MRSI) data from the tumor region, overlaid on the postcontrast T1. (B) Representative spectra from and around the enhancing lesion. (C) $MTV_{Cho}$ (blue), GTV (red) and edema (orange) overlaid on postcontrast T1 in axial, sagittal, and coronal views. MTV = metabolic tumor volumes. A color version of this figure available at www.redjournal.org.

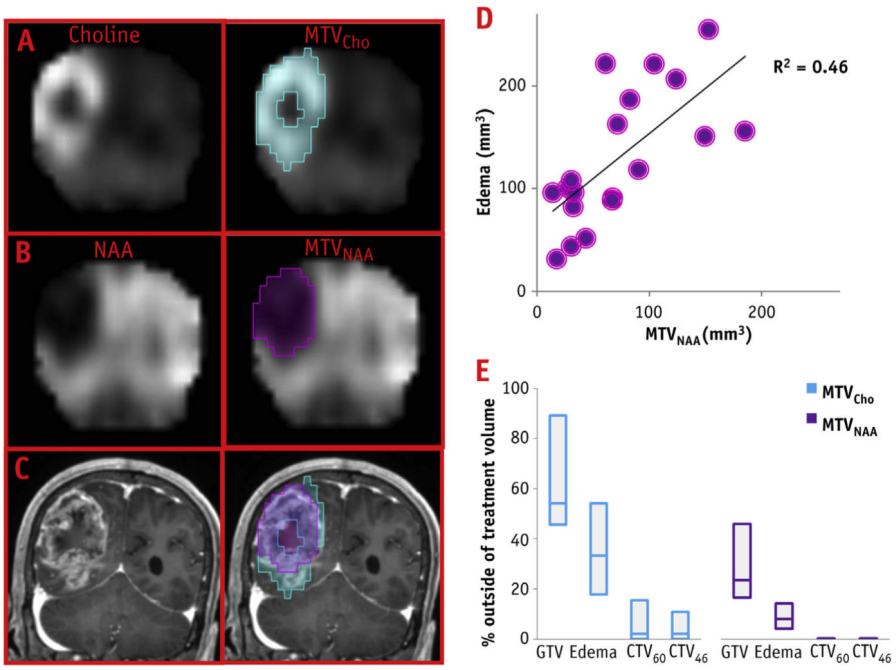


**Fig. 5.**

(A) Coronal view of choline (Cho) and $MTV_{Cho}$ (blue) maps. (B) *N*-acetylaspartate (NAA) and $MTV_{NAA}$ (purple). (C) $MTV_{Cho}$ and $MTV_{NAA}$ overlaid on post-contrast T1 MRI. (D) Correlation of $MTV_{NAA}$ and edema volumes. (E) Boxplot of the percentage of $MTV_{Cho}$ and $MTV_{NAA}$ outside of radiation therapy volumes. MTV Z metabolic tumor volumes.

*Int J Radiat Oncol Biol Phys*. Author manuscript; available in PMC 2015 October 01.

**Table 1**

Patient characteristics and summary of radiation treatment and metabolic volumes

| Patient ID | Age | Sex | Brain volume ($mm^3$) | RT volumes ($mm^3$) | | | | Metabolic volumes ($mm^3$) | | | % of $MTV_{Cho}$ outside of: | | | | % of $MTV_{NAA}$outside of: | |
|---|---|---|---|---|---|---|---|---|---|---|---|---|---|---|---|---|
| | | | | GTV | Edema | $CTV_{60}$ | $CTV_{46}$ | $MRSI_Q$ | $MTV_{Cho}$ | $MTV_{NAA}$ | GTV | Edema | $CTV_{60}$ | $CTV_{46}$ | GTV | Edema |
| T1* | 40 | M | 1341 | 24 | 151 | 280 | 415 | 989 | 27 | 150 | 99.8 | 50.9 | 0.3 | 0.0 | 83.8 | 20.6 |
| T2 | 53 | M | 1242 | 70 | 101 | 352 | 359 | 872 | 10 | 28 | 39.6 | 29.8 | 0.1 | 0.1 | 0.7 | 0.1 |
| T3 | 60 | F | 1297 | 31 | 44 | 187 | 157 | 922 | 37 | 31 | 51.0 | 39.7 | 0.0 | 0.0 | 22.8 | 14.2 |
| T4 | 60 | M | 1335 | 116 | 207 | 505 | 566 | 941 | 15 | 124 | 25.6 | 6.4 | 0.0 | 0.0 | 18.3 | 5.1 |
| T5 | 31 | F | 1122 | 20 | 31 | 188 | 176 | 798 | 20 | 18 | 84.2 | 76.5 | 21.9 | 23.2 | 20.2 | 7.0 |
| T6† | 47 | M | 1398 | 118 | 118 | 429 | 367 | 1067 | 104 | 91 | 24.7 | 24.7 | 0.1 | 0.1 | 9.0 | 9.0 |
| T7# | 30 | M | 1268 | 12 | 156 | 266 | 410 | 907 | 161 | 185 | 92.8 | 25.1 | 15.6 | 3.2 | 93.4 | 22.3 |
| T8 | 34 | M | 1406 | 31 | 187 | 350 | 590 | 1040 | 227 | 83 | 86.7 | 33.3 | 15.7 | 1.4 | 65.1 | 14.3 |
| T9 | 50 | M | 1377 | 24 | 52 | 312 | 276 | 1023 | 12 | 44 | 91.8 | 90.8 | 7.4 | 12.7 | 52.5 | 27.2 |
| T10 | 62 | F | 1188 | 43 | 91 | 310 | 347 | 893 | 16 | 68 | 54.3 | 46.6 | 21.3 | 20.8 | 39.4 | 8.1 |
| T11 | 38 | M | 1239 | 100 | 255 | 483 | 533 | 881 | 21 | 153 | 47.2 | 11.0 | 0.0 | 0.3 | 39.3 | 11.9 |
| T12 | 47 | M | 1439 | 61 | 89 | 409 | 396 | 1072 | 17 | 67 | 97.8 | 95.5 | 55.8 | 8.8 | 25.2 | 11.5 |
| T13 | 69 | M | 1322 | 59 | 163 | 371 | 451 | 978 | 2 | 72 | 100 | 100 | 100 | 86.5 | 30.5 | 2.1 |
| T14 | 66 | M | 1284 | 42 | 82 | 466 | 443 | 943 | 58 | 32 | 46.2 | 24.4 | 0.7 | 3.4 | 23.5 | 8.0 |
| T15§ | 41 | F | 1302 | 122 | 221 | 491 | 561 | 969 | 28 | 104 | 63.3 | 35.5 | 3.4 | 3.5 | 14.5 | 2.6 |
| T16 | 38 | M | 1497 | 14 | 96 | 279 | 365 | 1133 | 3 | 8 | 45.2 | 0.0 | 0.0 | 0.0 | 66.8 | 14.4 |
| T17 | 65 | F | 1079 | 75 | 96 | 280 | 296 | 768 | 35 | 33 | 64.3 | 57.3 | 10.4 | 17.0 | 9.9 | 6.1 |
| T18 | 47 | M | 1564 | 161 | 222 | 589 | 551 | 1153 | 19 | 61 | 5.5 | 5.5 | 2.0 | 2.0 | 4.6 | 3.1 |
| T19 | 50 | F | 1117 | 36 | 108 | 241 | 311 | 840 | 14 | 31 | 46.7 | 10.2 | 1.4 | 1.4 | 19.3 | 2.7 |
| **Median** | **47** | - | **1302** | **43** | **108** | **350** | **396** | **943** | **20** | **67** | **54.3** | **33.3** | **2.0** | **2.0** | **22.8** | **8.1** |
| **IQR** | **21** | - | **147** | **60** | **85** | **168** | **163** | **144.5** | **21.5** | **66** | **46.4** | **36.4** | **15.6** | **10.7** | **26.8** | **9.0** |

*Abbreviations:* Cho = choline; $CTV_{46}$ = clinical target volume, receiving radiation dose of 46 Gy ($CTV_{46}$ = edema + 2 cm); $CTV_{60}$ = clinical target volume, receiving radiation dose of 60 Gy ($CTV_{60}$ = GTV+2.5 cm); F = female; GTV = gross tumor volume; IQR = interquartile range (a measure of statistical dispersion, being equal to the difference between the upper [75th percentile] and lower [25th percentile] quartile); M = male; MRSI = magnetic resonance spectroscopic imaging; $MRSI_Q$ = volume of MRSI within the "quality mask"; MTV = metabolic tumor volume; $MTV_{Cho}$ = MTV, based on Cho values above estimated threshold; $MTV_{NAA}$ = MTV, based on NAA values below estimated threshold; NAA = *N*-acetylaspartate; RT = radiation therapy.

#Data from this patient are reviewed in detail in Figure 2.

* Data from this patient are reviewed in detail in Figure 3.

† Data from this patient are reviewed in detail in Figure 5.

§ Data from this patient are reviewed in detail in Figure 4.